MOX–Report No. 20/2010

Numerical solution of an active strain formulation for the electromechanical activity in the heart

FABIO NOBILE, ALFIO QUARTERONI, RICARDO RUIZ BAIER

Numerical solution of an active strain formulation for the electromechanical activity in the heart

Fabio Nobile[†], Alfio Quarteroni[†,♯] and Ricardo Ruiz Baier[♯]

June 15, 2010

[†] MOX– Modellistica e Calcolo Scientifico
Dipartimento di Matematica "F. Brioschi"
Politecnico di Milano
via Bonardi 9, 20133 Milano, Italy
[♯] CMCS– Modeling and Scientific Computing
Ecole Polytechnique Fédérale de Lausanne EPFL
Station 8, CH-1015, Lausanne, Switzerland
ricardo.ruiz@epfl.ch

Abstract

We propose a finite element method for solving a system of equations describing the coupling between cardiac mechanics and electrical signalling. The model is based on a multiplicative decomposition of the deformation tensor into a passive and active part, the latter carrying the information of the electrical potential propagation and anisotropy of the cardiac tissue into the equations of incompressible or nearly incompressible nonlinear elasticity, governing the mechanical response of the biological material. Moreover, by changing from an Eulerian to a Lagrangian configuration, the underlying problem exhibits a nonlinear diffusion term in the equations of the electrical propagation (namely, the bidomain and monodomain equations). Piecewise quadratic finite elements are used to approximate the displacements field, while for pressure, electrical potentials and ionic variables, we use piecewise linear elements. Various test cases show that the proposed method is able to capture some important features of the studied phenomenon, and illustrate the behavior of the global model.

1

1   Introduction

This work deals with the numerical simulation of the interaction between the propagation of electrical potential and large deformations of the cardiac tissue. This subject has gained a considerable attention in recent years, as shown by the increasing number of contributions in applied mathematics and bioengineering (see e.g. [7, 22, 23, 29], the list being far from complete). The diversity of these studies suggests that both the modeling and numerical treatment of this class of problems is far from being a resolved subject. A considerable amount of literature is available for the much more established understanding of a particular facet of the problem, namely the mechanisms that drive the electrophysiological activity in the heart. Several numerical methods have been proposed and analyzed for efficiently solving the Bidomain and Monodomain equations (see e.g. [8, 31, 35]).

In this paper we shortly illustrate a recently proposed model for cardiac electromechanics, and we introduce a suitable numerical method for its approximation. More precisely, the main ingredients include a modeling of the excitation-contraction mechanism based on the recent description of [1, 7]. The deformation of the tissue can be modeled assuming a quasi-steady elasticity framework, in which we suppose that a multiplicative decomposition between the active and passive mechanical response can be introduced at the deformation level. In this context we consider that the active part of the mechanical response carries the information about the anisotropy of the tissue through the fibers' orientation. The main features of this model are essentially derived from the electromechanical model of a one-dimensional fiber. Despite some necessary simplifications in the underlying physics, the proposed model is able to address the main features of the complete mechanical/electro-dynamical system, providing more insight on the role of the active strain in the cardiac electromechanical phenomenon. Our framework can of course accommodate the study of more general material properties, such as ortothropy, and different model parameters. Another goal of this paper is to introduce a suitable finite element method for obtaining accurate numerical approximations of our coupled problem, and to present some numerical examples to illustrate the behavior of the phenomenon. In this work we will restrict to consider a weak coupling between the mechanical response and electrical propagation.

The remainder of this paper is organized as follows. In Section 2, the bidomain model for the electrical activity is outlined, followed by a description of an appropriate mechanical framework on the basis of finite elasticity. Next, we give a precise meaning to the coupling between mechanics and electrical activity in the tissue. In Section 3 we construct the corresponding finite element method to solve the derived coupled problem, and Section 4 contains several numerical examples putting into evidence the good behavior of the models and methods proposed. Finally, some conclusions are drawn in Section 5.

2   Formulation of the electromechanical problem

A contraction of the cardiac muscle generally takes place in response to an electrical impulse. On the other hand, it is known that myocardial stretch can cause changes in the electrophysiological properties of the heart (mechano-electrical feedback). As a matter of fact, several experimental

studies both in vitro and in vivo, have proved that the myocardial stretch is responsible for the change in the configuration of action potential, which leads to afterdepolarization-like activity and arrhythmias (see e.g. [27]). In short, the cardiac electromechanical response behaves as follows. An electrical impulse starts in the sinoatrial node. There, a depolarization begins and a wave propagates across the atria, followed by a delay of the potential at the atrioventricular node. Then a rapid depolarization of both ventricles occurs, which at the cellular level causes an increasing of calcium concentration, and this mechanism produces a contraction by a temporary binding between actin and myosin. This complex mechanism has been studied since many years. We will focus the study on the macroscopic part of the coupling. In the following, we will divide the description into three main parts: the equations governing the electrical activity, the equations for the mechanical behavior of the tissue, and finally the coupling strategy.

In order to consider each sub-problem in a natural approach, we will formulate both the electrical propagation and the nonlinear mechanics in a pure Lagrangian framework. To this end, by $\Omega_o \subset \mathbb{R}^3$ we will denote the bounded spatial domain in the undeformed equilibrium state.

2.1 The governing equations for the electrical model

The quantities of interest in the Bidomain model for electrical signaling in the heart, are the *intracellular* and *extracellular* electric potentials, $u_i = u_i(\mathbf{X}, t)$ and $u_e = u_e(\mathbf{X}, t)$, at $(\mathbf{X}, t) \in \Omega_T := \Omega_o \times (0, T)$. Their difference $v = v(\mathbf{X}, t) := u_i - u_e$ is the transmembrane potential. The conductivity of the tissue is represented by scaled tensors $\mathbf{D}_i(\mathbf{X})$ and $\mathbf{D}_e(\mathbf{X})$, that, under axial symmetry, are given by

$$\mathbf{D}_k(\mathbf{X}) = \sigma_k^t \mathbf{I} + \left(\sigma_k^l - \sigma_k^t\right) \boldsymbol{a}_l(\mathbf{X}) \boldsymbol{a}_l^T(\mathbf{X}), \quad k \in \{e, i\},$$

where $\sigma_k^l = \sigma_k^l(\mathbf{X}) \in C^1(\mathbb{R}^3)$ and $\sigma_k^t = \sigma_k^t(\mathbf{X}) \in C^1(\mathbb{R}^3)$, $k \in \{e, i\}$, are the intra- and extracellular conductivities along and transversal to the direction of the fiber (parallel to the unitary direction vector denoted by $\boldsymbol{a}_l(\mathbf{X})$), respectively, and $\boldsymbol{a}_t(\mathbf{X})$ its transpose. This description is crucial in the model, since the cardiac tissue is actually made of fibers that drive the propagation of the electrical potential. Even if the fibers' distribution is rather known (subepicardial myofibers follow a left-handed helix parallel to the wall, crossing the wall near the apex, and then continue in a right-handed helical pathway at the subendocardium; the fibers cross over to the subepicardium near the base), some simplifications can be assumed, for example, that fibers are aligned with the domain axis, in which case we have that $\mathbf{D}_i(\mathbf{X})$ and $\mathbf{D}_e(\mathbf{X})$ are diagonal matrices: $\mathbf{D}_i(\mathbf{X}) = \text{diag}(\sigma_i^l, \sigma_i^t, \sigma_i^t)$ and $\mathbf{D}_e(\mathbf{X}) = \text{diag}(\sigma_e^l, \sigma_e^t, \sigma_e^t)$. In terms of physiological relevance, an intermediate description allows that the fibers are aligned to the fixed angle θ. Then $\mathbf{D}_k$ is recast explicitly in the form

$$\mathbf{D}_k = \begin{bmatrix} \sigma_k^t + (\sigma_k^l - \sigma_k^t)\cos^2(\theta) & (\sigma_k^l - \sigma_k^t)\sin(\theta)\cos(\theta) & 0 \\ (\sigma_k^l - \sigma_k^t)\sin(\theta)\cos(\theta) & \sigma_k^t + (\sigma_k^l - \sigma_k^t)\sin^2(\theta) & 0 \\ 0 & 0 & \sigma_k^t \end{bmatrix},$$

for $k \in \{e, i\}$. The conductivities in the longitudinal direction must be larger than in the transversal direction.

3

The bidomain model is given by the following coupled reaction-diffusion system (for a general introduction, see e.g. [31]):

$$\chi c_{\mathrm{m}} \partial_t v - \nabla \cdot \left(\mathbf{D}_{\mathrm{i}}(X) \nabla u_{\mathrm{i}}\right) + \chi I_{\mathrm{ion}}(v, \boldsymbol{w}) = 0,$$
$$\chi c_{\mathrm{m}} \partial_t v + \nabla \cdot \left(\mathbf{D}_{\mathrm{e}}(X) \nabla u_{\mathrm{e}}\right) + \chi I_{\mathrm{ion}}(v, \boldsymbol{w}) = I_{\mathrm{app}}, \tag{2.1}$$
$$\partial_t \boldsymbol{w} - H(v, \boldsymbol{w}) = 0, \qquad (X, t) \in \Omega_T,$$

provided with homogeneous Neumann boundary conditions. Here, $c_{\mathrm{m}} > 0$ is the *surface capacitance* of the membrane, χ is the ratio of membrane area per tissue volume, and $\boldsymbol{w}(X, t)$ is the *gating* variable, which controls the local repolarization behavior of the action potential and it is scalar or vectorial, depending on the choice of membrane model. The knowledge of suitable initial conditions for $v, u_{\mathrm{e}}, \boldsymbol{w}$ is also required. The stimulation current possibly applied to the extracellular space is represented by the function $I_{\mathrm{app}} = I_{\mathrm{app}}(X, t)$. In the case that $\mathbf{D}_{\mathrm{i}} = \varrho \mathbf{D}_{\mathrm{e}}$ for some $\varrho \in \mathbb{R}$, the bidomain system reduces to the *monodomain model*:

$$\chi c_{\mathrm{m}} \partial_t v - \nabla \cdot \left(\frac{\mathbf{D}_{\mathrm{i}}(X)}{1 + \varrho} \nabla v\right) + \chi I_{\mathrm{ion}}(v, \boldsymbol{w}) = \frac{\varrho}{1 + \varrho} I_{\mathrm{app}},$$
$$\partial_t \boldsymbol{w} - H(v, \boldsymbol{w}) = 0, \qquad (X, t) \in \Omega_T. \tag{2.2}$$

This simpler model requires less computational effort than (2.1), and even though the assumption of equal anisotropy ratios is very strong and generally unrealistic, (2.2) is still adequate for a qualitative investigation of certain repolarization sequences and the distribution of patterns of durations of the action potential [8].

The choice of the functions $H(v, \boldsymbol{w})$ and $I_{\mathrm{ion}}(v, \boldsymbol{w})$ is determined by the membrane model to be used. Depending on the level of complexity of the type problem to be studied, we will restrict ourselves to two membrane models. First, the Rogers-McCulloch model [28], which is based on purely phenomenological evidence, and is given by

$$H(v, \boldsymbol{w}) = bv - \boldsymbol{w},$$
$$I_{\mathrm{ion}}(v, \boldsymbol{w}) = c_2 v \boldsymbol{w} - c_1 v(1 - v)(v - a), \tag{2.3}$$

where a, b, c_1, c_2 are model parameters. Even though very simple, this model is able to capture the characteristic shape of the action potential curve (see Figure 1 top). The phase diagram in Figure 1-bottom shows computed trajectories for different initial values of v_0 and $\boldsymbol{w}_0$ which converge to the stable equilibrium state $(0, 0)$. In order to provide results on a physiologically more accurate scale for electrical potentials and time, the RM model (2.3) will be conveniently replaced by

$$H(v, w) = \frac{b}{TA}(v - v_{\mathrm{min}} - Aw),$$
$$I_{\mathrm{ion}}(v, w) = \frac{c_1}{TA^2}(v - v_0)(v - v_{\mathrm{min}} - aA)(v - v_{\mathrm{min}} - A) + \frac{c_2}{T}(v - v_{\mathrm{min}})w. \tag{2.4}$$

The right column of Figure 1 displays the corresponding action potential curves and phase diagram. Secondly, we use the phase-I Luo-Rudy (LRI) model [20] constructed on the basis of a description of ionic currents. In that model, $\boldsymbol{w}$ is a vector of dimensionless ion-channel gating variables, and
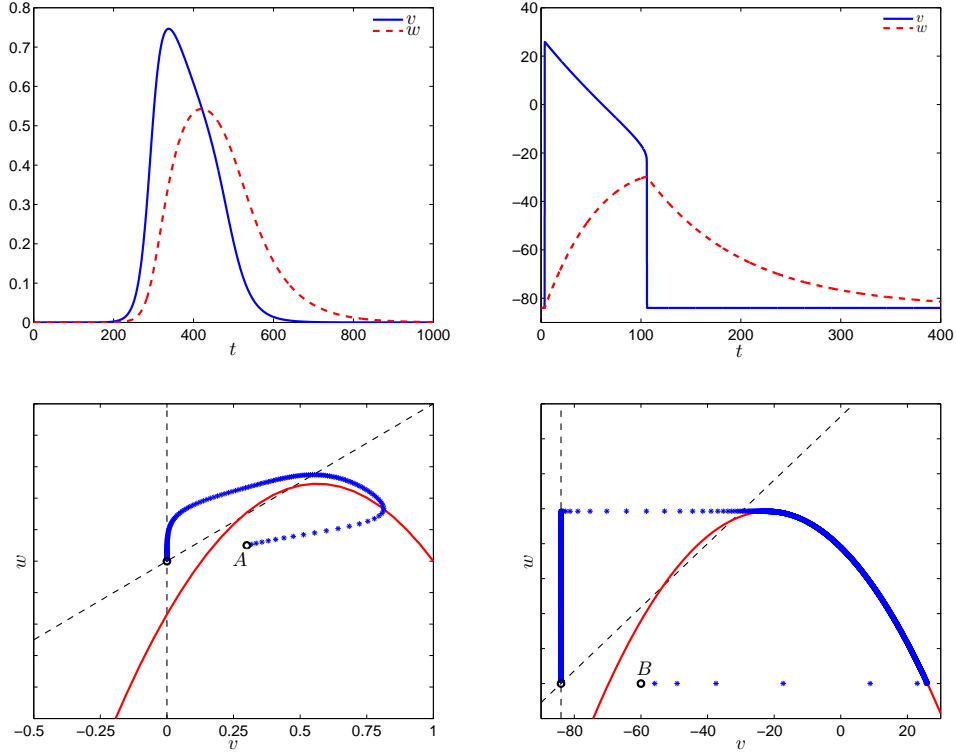
Figure 1: Action potential curve (top) and phase portrait (bottom) for the Rogers-McCulloch model in the original (left) and rescaled (right) case, starting from the initial states $A = (0.3, 0.1)$, $B = (-60, 0)$ and reaching the intersections of the nullclines.

the total ionic current density $I_{\mathrm{ion}}(v, \boldsymbol{w})$ is the sum of a fast inward sodium current I_{Na}, a slow inward current I_{si}, a time-dependent potassium slow outward current I_{K}, an outward potassium current $I_{\mathrm{K_1}}$, a plateau potassium current $I_{\mathrm{K_p}}$, and a total background current I_{b}. For completeness, further details are provided in the Appendix.

2.2 Model for finite elasticity

The myocardium is composed of connective tissue and cells surrounded by space filled with fluid, all of these materials being mainly formed by water. From the mechanical viewpoint, the heart tissue in its resting state can be regarded as an inhomogeneous, anisotropic, and incompressible (or nearly incompressible) elastic material [13]. The tissue is subject to external load and active deformation inducing a strain field. An adequate scenario for the modeling of cardiac mechanics is then provided by the nonlinear elasticity framework.

From now on, $\boldsymbol{x}$ will denote the current position of a particle that occupied the position $\mathbf{X}$ in

the initial undeformed configuration, and $\boldsymbol{d} = \boldsymbol{x} - \mathbf{X}$ stands for the displacement field. Then

$$\mathbf{F} = \nabla \boldsymbol{x} = \mathbf{I} + \nabla \boldsymbol{d}, \quad F_{ij} = \frac{\partial x_i}{\partial X_j} = \delta_{ij} + \frac{\partial d_i}{\partial X_j},$$

where δ_{ij} denotes the Kronecker delta, is the deformation gradient tensor, measuring strain between the deformed and undeformed states. The symbol ∇ denotes the gradient of a quantity with respect to the material coordinates $\mathbf{X}$. We assume that $\mathbf{F}$ can be decomposed (factorized) into an elastic (passive) factor taking place at a macroscale, and an active factor, acting at the microscale (see e.g. [21])

$$\mathbf{F} = \mathbf{F}_e \mathbf{F}_o. \tag{2.5}$$

Notice that $\mathbf{F}$ is given by the gradient of a vector map, while $\mathbf{F}_e, \mathbf{F}_o$ are not, in general. In the sequel we will refer to this setting as the *active strain* formulation. Similar decompositions have been proposed in the context of finite elastoplasticity (see e.g. [30]).

By J, J_o we denote the determinants of $\mathbf{F}, \mathbf{F}_o$, respectively. The Jacobian J describes the volume map of infinitesimal reference elements onto the corresponding current elements. In other electromechanical models available (see e.g. [23, 22, 29]), an appropriate term is added to the passive stress tensor, generating an additive decomposition between passive and active stress. We will refer to the latter decomposition as *active stress* formulation. It is demonstrated in [21] that the active stress decomposition is equivalent to (2.5) only in the special case of small deformations. A deeper discussion on the active stress vs. active strain formulations can be also found in [1].

As discussed in [36], the time-space scales in the cardiac electromechanical phenomenon suggest the use of steady state equations of motion to describe the conservation of linear and angular momentum. These are reduced to the force balance

$$-\nabla \cdot \mathbf{P} = \boldsymbol{f},$$

where $\mathbf{P}$ is the Piola-Kirchoff stress, which represents force per unit undeformed surface, and $\boldsymbol{f}$ is a vector of body forces. Note that the balance is defined in the undeformed state Ω_o.

The definition of $\mathbf{P}$ in terms of the components of the deformation stress and strain measures, is given by the constitutive relations. In the studied context, the medium is typically assumed to be an hyperelastic material. Therefore it can be postulated that there exists an elastic strain energy density function $\mathcal{W} = \mathcal{W}(\mathbf{F}_e)$ depending only on the present value of the elastic deformation, which characterizes the material. Among the wide variety of models that have been proposed for the passive cardiac tissue (for an updated review on this aspect, we refer the reader to [13]), we consider simple Mooney-Rivlin materials, for which the internal stored energy function reads

$$\mathcal{W}(\mathbf{F}_e) = \frac{\mu_1}{2} \big(\text{tr}(\mathbf{F}_e \mathbf{F}_e^T) - 3 \big) + \frac{\mu_2}{4} \big((\text{tr}(\mathbf{F}_e \mathbf{F}_e^T))^2 - \text{tr}(\mathbf{F}_e \mathbf{F}_e^T)^2 - 6 \big),$$

where μ_1, μ_2 are elastic moduli. For Neo-Hookean materials $\mu_2 = 0$. To assure incompressibility of the material (where only isochoric behavior is allowed), the strain energy is assumed to take the form

$$\mathcal{W}^{\text{iso}} = \mathcal{W}(\mathbf{F}_e) + p(J - 1),$$

where p is the Lagrange multiplier arising from the imposition of the incompressibility constraint $J = 1$ (conservation of mass), and which is usually interpreted as the hydrostatic pressure field.

The Piola-Kirchoff stress tensor is given by the Frechet derivative of the internal stored energy function $\mathcal{W}$, which in the fully relaxed configuration reads

$$\mathbf{P} = J_o \frac{\partial \mathcal{W}}{\partial \mathbf{F}_e} \mathbf{F}_o^{-T} - p \mathbf{F}_e^{-T} \mathbf{F}_o^{-T},$$

where for Mooney-Rivlin materials it takes the form

$$\mathbf{P} = J_o \big(\mu_1 + \mu_2 \mathrm{tr}(\mathbf{F}\mathbf{F}_o^{-1}\mathbf{F}_o^{-T}\mathbf{F}^T) \big) \mathbf{F}\mathbf{F}_o^{-1}\mathbf{F}_o^{-T} - \mu_2 J_o \big(\mathbf{F}\mathbf{F}_o^{-1}\mathbf{F}_o^{-T}\mathbf{F}^T \big)^2 \mathbf{F}^{-T} - p \mathbf{F}^{-T}.$$

An alternative step is to consider *nearly incompressible* materials to avoid solving a mixed-type problem. In such case, a strain energy function for Neo-Hookean materials is (see [5, 14])

$$\mathcal{W}(\mathbf{F}_e) = \frac{\mu_1}{2} \big(\mathrm{tr}(\mathbf{F}_e \mathbf{F}_e^T) - 3 - 2\ln(J) \big).$$

The discussion on whether the myocardium should be modeled as incompressible or nearly incompressible is apparently not resolved, we therefore leave the door open for considering both approaches.

We point out that if the chosen strain energy function has desirable stability properties (such as polyconvexity and coercivity), then the application of an active strain decomposition like (2.5) essentially traduces into a simple *shift* of the relaxation state from $\mathbf{I}$ to $\mathbf{F}_o^{-1}$, therefore preserving the qualitative structure of $\mathcal{W}$. In this sense, the active strain formulation could be straightforwardly extended to the study of more adequate material models, like the structurally based model for the passive properties of the cardiac tissue presented in [13]. Notice that in the material law used herein, so far we have not addressed a major ingredient in the modeling of cardiac dynamics which is anisotropy. Obviously, the strain energy could also be considered to depend explicitly on the fibers distribution through the inclusion of further invariants of the left Cauchy-Green tensor, or through the use of components of the Green-Lagrange strain tensor, as in e.g. [15, 23, 32].

In contrast, we propose to account for the anisotropic behavior of the fibers simply by assigning direction-specific active deformation fields in the active part of the decomposition. More specifically, for a myofiber distribution along the direction of the unit vectors $\boldsymbol{a}_l, \boldsymbol{a}_t$, we consider that the active strain assumes the form

$$\mathbf{F}_o = \mathbf{I} + \gamma_l \boldsymbol{a}_l \otimes \boldsymbol{a}_l + \gamma_t \boldsymbol{a}_t \otimes \boldsymbol{a}_t, \tag{2.6}$$

where $\boldsymbol{a}_l, \boldsymbol{a}_t$ are the fiber sheet longitudinal and transversal directions respectively (which in a simplified setting are assumed to represent fixed directions, for any point $\mathbf{X}$), and γ_i are scalar fields accounting for the activation, depending on macroscopic stimuli related to the electrical part of the model, which will be made precise later. Recently, in [12] the authors also use an anisotropic contribution in the active part of the cardiac response, but this is included in the framework of an active stress formulation. We point out that our approach is not necessarily incompatible with an

anisotropic description at the passive elastic level (which will give a more physiologically relevant mechanical description), however we leave such analysis for a future study.

Putting together the previous description, we obtain that the Euler-Lagrange problem (in its weak formulation) reads: Find $\boldsymbol{d}, p$ in suitable admissible displacement and pressure spaces such that

$$\int_{\Omega_o} \left(\mu_1 J_o (\mathbf{I} + \nabla \boldsymbol{d}) \mathbf{F}_o^{-1} \mathbf{F}_o^{-T} : \nabla \boldsymbol{\varphi} - pJ (\mathbf{I} + \nabla \boldsymbol{d})^{-T} : \nabla \boldsymbol{\varphi} \right) = 0$$

$$\int_{\Omega_o} (J - 1) q = 0, \tag{2.7}$$

for all test functions $\boldsymbol{\varphi}, q$. Concerning boundary conditions, we have proceeded by specifying a displacement field on a portion Γ_D of $\partial \Omega_o$, which for simplicity has been taken as homogeneous Dirichlet boundary data

$$\boldsymbol{d} = \boldsymbol{0} \qquad \text{on } \Gamma_D \subset \partial \Omega_o, \tag{2.8}$$

and homogeneous Neumann conditions on $\partial \Omega_o \setminus \Gamma_D$.

2.3 The coupled model

With the purpose to study the basic mechanisms of the mechano-electrical feedback, and the related numerical challenges, we herein consider a rather simple cupled model. We first assume that the active deformation functions γ_i, $i = l, t$ (Figure 2) depend directly on the transmembrane potential through the following sublinear relation (see also [1], where a linear dependence with the transmembrane potential is proposed)

$$\gamma_l(v) = -\sigma_l \beta \frac{v - v_{\min}}{v_{\max} - v_{\min} + v}, \quad \gamma_t(v) = -\sigma_t \beta \frac{v - v_{\min}}{v_{\max} - v_{\min} + v}, \tag{2.9}$$

where $v_{\min}, v_{\max}$ are problem-dependent parameters accounting for the proper scaling of the solution, $\beta = 0.3$ is included to model the change of length experimented by the cardiac fibers in a normal heartbeat, and σ_l, σ_t are the conductivity factors defined in Section 2.1. Notice that the definition of γ implies that the ratio between the intensity of the contraction in each direction of the fiber with respect to the other direction coincides with the corresponding conductivity ratio. In the light of (2.6), $\gamma < 0$ implies a contraction of the myocardium. This approach then assumes that the information of the electrical part of the model enters in the mechanical description through (2.6),(2.9) only. To account for the coupling at the microscale, we also relate the activation function γ to the intracellular calcium concentration $[\mathrm{Ca}]_+$ in the following way (see the similar model in [7]):

$$\gamma_i(v, [\mathrm{Ca}]_+) = -\sigma_i \beta \frac{v - v_{\min}}{v_{\max} - v_{\min} + v} + \varepsilon_i \beta \frac{l_o^i}{1 + \eta([\mathrm{Ca}]_+)(l_o^i - 1)},$$

for $i = l, t$, where $l_o^i = (\eta(c_o^*) - \varepsilon_i)^{-1}(\eta(c_o^*) - 1)$, $\eta([\mathrm{Ca}]_+) = \frac{1}{2} + \frac{1}{\pi} \arctan(\beta^2 \log([\mathrm{Ca}]_+/c_R))$, and $c_o^*, c_R, \varepsilon_i$ are given parameters. We will use this approach only when a ionic model (such as Luo-Rudy) is considered. For simplified membrane models (Rogers-McCulloch), the terms γ_i are
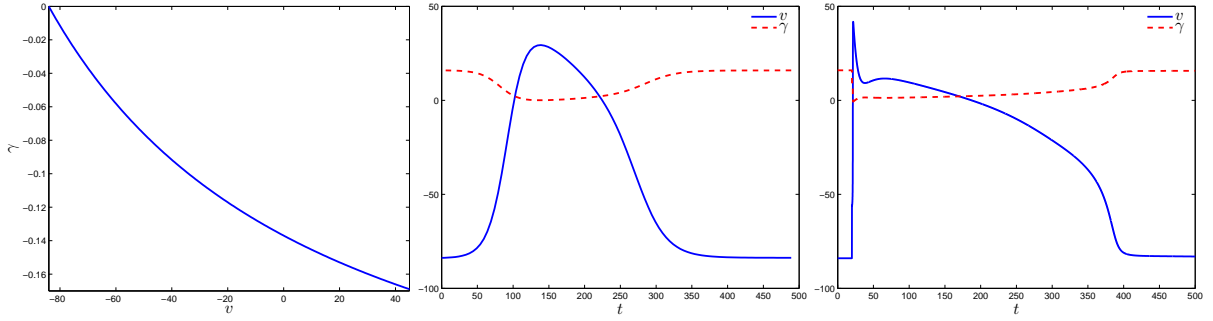
8

Figure 2: Mean active deformation function $\gamma = \dfrac{\gamma_l + \gamma_t}{2}$ (a measure of the bulk active strain) depending on the transmembrane potential (left), action potential curve and active deformation function during a $500\,\mathrm{ms}$ period for the Rogers-McCulloch and Luo-Rudy I models (middle and right, respectively).

taken as in (2.9). A more accurate description is indeed possible by considering a detailed model of the microscopic activation depending on more involved elements of the ionic activity, such as specific sarcomere length (as done for instance in [27, 29]), but we restrict ourselves to the present simpler setting.

The second main ingredient of the electromechanical coupling is the proper representation of the dependence of the electrical properties of the tissue, on the active strain. One approach to account for the influence of the mechanical response into the electrophysiology, is essentially provided by a transformation of coordinates from Eulerian to Lagrangian and the use of the Piola identity $\nabla \cdot (J\mathbf{F}^{-T}) = 0$ (see details in [1]). Other related approaches (to be included in a forthcoming analysis) are based on a dependence of ionic currents, on certain microscopic mechanical processes (see [29, 32]).

Collecting the items of the analysis above, and considering for instance, the case of incompressible Neo-Hookean materials, we end up with the following bidomain electromechanical coupled model

$$
\begin{aligned}
-\nabla \cdot \left(\mu_1 J_o(\mathbf{I} + \nabla \boldsymbol{d})\mathbf{F}_o^{-1}\mathbf{F}_o^{-T} - p(\mathbf{I} + \nabla \boldsymbol{d})^{-T} \right) &= 0 \quad && \text{in } \Omega_o, \\
J &= 1 \quad && \text{in } \Omega_o, \\
\chi c_\mathrm{m} \partial_t v - \nabla \cdot \left(J_o(\mathbf{I} + \nabla \boldsymbol{d})^{-1}\mathbf{D}_\mathrm{e}(\mathbf{I} + \nabla \boldsymbol{d})^{-T}\nabla u_\mathrm{e} \right) + \chi I_\mathrm{ion} &= 0 \quad && \text{in } \Omega_T, \\
\chi c_\mathrm{m} \partial_t v + \nabla \cdot \left(J_o(\mathbf{I} + \nabla \boldsymbol{d})^{-1}\mathbf{D}_\mathrm{i}(\mathbf{I} + \nabla \boldsymbol{d})^{-T}\nabla u_\mathrm{i} \right) + \chi I_\mathrm{ion} &= I_\mathrm{app} \quad && \text{in } \Omega_T, \\
\partial_t \boldsymbol{w} - H(v, \boldsymbol{w}) &= 0 \quad && \text{in } \Omega_T.
\end{aligned}
$$

$$(2.10)$$

The system of equations has to be completed with no-flux boundary conditions for the electric variables, Dirichlet boundary conditions for the mechanical balance equation, and suitable initial data for $u_\mathrm{e}, v, \boldsymbol{w}$.

Analogously, we have the monodomain electromechanical system (written in terms of $v, p, \mathbf{X}$):

$$-\nabla \cdot \left(\mu_1 J_o (\mathbf{I} + \nabla \boldsymbol{d}) \mathbf{F}_o^{-1} \mathbf{F}_o^{-T} - p(\mathbf{I} + \nabla \boldsymbol{d})^{-T} \right) = 0 \quad \text{in } \Omega_o,$$
$$J = 1 \quad \text{in } \Omega_o,$$
$$\partial_t v - \nabla \cdot \left(J_o (\mathbf{I} + \nabla \boldsymbol{d})^{-1} \mathbf{D} (\mathbf{I} + \nabla \boldsymbol{d})^{-T} \nabla v \right) = I_{\text{ion}}(v, \boldsymbol{w}) \quad \text{in } \Omega_T,$$
$$\partial_t \boldsymbol{w} - H(v, \boldsymbol{w}) = 0 \quad \text{in } \Omega_T. \tag{2.11}$$

Note that the third equation is a balance equation for the potential, accounting for the dynamics between flow and reactions of ionic species, whereas the last equation is pointwise attached to the material and does not represent any balance in space. Note also that (2.10) and (2.11) are both written in the total Lagrangian formulation, that is, only in terms of the undeformed configuration.

2.4   Weak formulation

Assuming that all unknowns are regular enough (we suppose $v, u_e \in L^2(0, T; H^1(\Omega_o))$, $w \in L^2(0, T, L^2(\Omega_o))$, $\boldsymbol{d} \in L^2(0, T; H_D^1(\Omega_o)^3)$, $p \in L_0^2(\Omega_o)$, in order to get bounded energy integrals), we multiply the equations in (2.10) by a vectorial test field $\boldsymbol{\varphi}$ vanishing on Γ_D, and by scalar test functions q, ξ^1, ξ^2, ξ^3 respectively. The weak problem associated to the coupled electromechanical model (2.10) reads as follows. Given $v_0, w_0 \in L^2(\Omega_o)$, $I_{\text{app}} \in L^2(\Omega_T)$, for $t \in (0, T)$, find a displacement vector $\boldsymbol{d}$, pressure p, electrical potentials v, u_e and ionic variables $\boldsymbol{w}$ such that the following identities hold for all test functions $\boldsymbol{\varphi}, q, \xi^j$:

$$\mu_1 \int_{\Omega_o} J_o (\mathbf{I} + \nabla \boldsymbol{d}) \mathbf{F}_o^{-1} \mathbf{F}_o^{-T} : \nabla \boldsymbol{\varphi} - \int_{\Omega_o} p(\mathbf{I} + \nabla \boldsymbol{d})^{-T} : \nabla \boldsymbol{\varphi} = 0,$$

$$\int_{\Omega_o} (J - 1) q = 0,$$

$$\int_{\Omega_o} \chi c_{\text{m}} \partial_t v \xi^i + \int_{\Omega_o} (\mathbf{I} + \nabla \boldsymbol{d})^{-1} \mathbf{D}_i (\mathbf{I} + \nabla \boldsymbol{d})^{-T} \nabla u_i \cdot \nabla \xi^i + \chi \int_{\Omega_o} I_{\text{ion}} \xi^i = 0,$$

$$\int_{\Omega_o} \chi c_{\text{m}} \partial_t v \xi^e - \int_{\Omega_o} (\mathbf{I} + \nabla \boldsymbol{d})^{-1} \mathbf{D}_e (\mathbf{I} + \nabla \boldsymbol{d})^{-T} \nabla u_e \cdot \nabla \xi^e + \chi \int_{\Omega_o} I_{\text{ion}} \xi^e = \int_{\Omega_o} I_{\text{app}} \xi^e,$$

$$\int_{\Omega_o} \partial_t \boldsymbol{w} \xi = \int_{\Omega_o} H \xi.$$

Although the wellposedness analysis of the bidomain equations for a (restricted) class of membrane models has received several recent contributions (see [4, 6, 9, 33]), the mathematical analysis of the cardiac mechanical response has been much less studied (see [10, 17]). As for the electromechanical coupling, it seems that there are no available results in terms of wellposedness and stability of solutions. For the model proposed herein, an analysis of existence (and uniqueness, under additional regularity restrictions on the mechanical variables) of solution, along with the stability of the coupled system is currently under development [3].

3 Finite element approximation

In this section, we outline the numerical strategy adopted to discretize the previously described model, and to obtain the corresponding approximate solutions.

Let $(0, T)$ be partitioned into $\tilde{N}$ subintervals $[t^n, t^{n+1}]$ of constant time step $\Delta t = t^{n+1} - t^n$ and denote with a superscript n the quantities computed at time t^n. Define $I_{\text{ion}}^{n+1} = I_{\text{ion}}(v^n, \boldsymbol{w}^{n+1})$. Then the semidiscrete system related to (2.10) reads as follows: Find $(\boldsymbol{d}, u_e, v, \boldsymbol{w})^{n+1}$ such that for all $n \in \{1, \ldots, \tilde{N}\Delta t\}$

$$\int_{\Omega_o} \mu_1 J_o^n (\mathbf{I} + \nabla \boldsymbol{d}^{n+1})(\mathbf{F}_o^n)^{-1}(\mathbf{F}_o^n)^{-T} : \nabla \boldsymbol{\varphi} - \int_{\Omega_o} p^{n+1}(\mathbf{I} + \nabla \boldsymbol{d}^{n+1})^{-T} : \nabla \boldsymbol{\varphi} + \int_{\Omega_o} (J^{n+1} - 1)q = 0,$$
$$(3.1)$$

$$\frac{\chi C_{\text{m}}}{\Delta t} \int_{\Omega_o} (v^{n+1} - v^n)\xi^i - \int_{\Omega_o} (\mathbf{I} + \nabla \boldsymbol{d}^{n+1})^{-1}\mathbf{D}_{\text{i}}(\mathbf{I} + \nabla \boldsymbol{d}^{n+1})^{-T}\nabla u_{\text{i}}^{n+1} \cdot \nabla \xi^i + \chi \int_{\Omega_o} I_{\text{ion}}^{n+1}\xi^i = 0,$$
$$(3.2)$$

$$\frac{\chi C_{\text{m}}}{\Delta t} \int_{\Omega_o} (v^{n+1} - v^n)\xi^e - \int_{\Omega_o} (\mathbf{I} + \nabla \boldsymbol{d}^{n+1})^{-1}\mathbf{D}_{\text{e}}(\mathbf{I} + \nabla \boldsymbol{d}^{n+1})^{-T}\nabla u_{\text{e}}^{n+1} \cdot \nabla \xi^e$$
$$+ \chi \int_{\Omega_o} (I_{\text{ion}}^{n+1} - I_{\text{app}}^{n+1})\xi^e = 0,$$
$$(3.3)$$

$$\frac{1}{\Delta t} \int_{\Omega_o} (\boldsymbol{w}^{n+1} - \boldsymbol{w}^n)\xi - \int_{\Omega_o} H(v^n, \boldsymbol{w}^{n+1})\xi = 0,$$
$$(3.4)$$

and a similar system is provided, corresponding to the semidiscrete counterpart for (2.11). Analogously to other approaches for the numerical treatment of the electromechanical coupling (as e.g. [15, 22, 23]), here we assume that the evolution of the macroscopic mechanical dynamics has a weak impact on the microscopic electrical activity, allowing in this way a formal uncoupling of the two sub-problems. Then, in practice, the fully coupled problem will be solved in a segregated way, and applying a standard backward Euler time integration scheme for ionic variables. However, further efforts are being made to include a monolithic treatment of the coupling, as done in [12]. A summary of the time-stepping algorithm is as follows: Assume that all field variables are known at time t^n. Then

i) The displacements $\boldsymbol{d}^{n+1}$ and pressure p^{n+1} are computed from (3.1) (see details in Section 3.1).

ii) The ionic variables $\boldsymbol{w}^{n+1}$ are obtained from (3.4).

iii) The electrical potentials $v^{n+1}, u_{\text{e}}^{n+1}$ are determined by solving (3.2)-(3.3).

As for the spatial discretization, we partition the domain Ω_o using a regular mesh $\mathcal{T}_h$ constructed by closed triangles (or tetrahedra for the 3D case) with boundary ∂K and diameter h_K. The mesh

parameter is $h = \max_{K \in \mathcal{T}_h}\{h_K\}$ and we use classical finite element spaces V_h^r approximating $H^1(\Omega_o)$ by piecewise polynomials of maximum order r on $\mathcal{T}_h$. More precisely,

$$V_h^r = \{v \in H^1(\Omega_o) \cap C^0(\overline{\Omega_o}) : v|_K \in \mathbb{P}_r(K) \text{ for all } K \in \mathcal{T}_h\},$$

for which $\{\varphi_h^r\}$ is a basis. It is evident that we are dealing with a saddle-point type problem. Then for the scheme to formally satisfy the discrete inf-sup or Ladyzhenskaya-Babuska-Brezzi stability condition (see e.g. [26]), the displacement field will be approximated using the FE space V_h^2, while the pressure (in the incompressible formulation) and electrical potential fields, will be approximated using V_h^1, other options being certainly possible (see [24] for a comparison of several discretization methods applied to soft tissue mechanics). The linear systems associated to the segregated bidomain (or monodomain) and ionic sub problems, are solved using a preconditioned GMRES iterative method (with LU preconditioner). On the other hand, the linear systems involved in the Newton step associated to the seggregated mechanical problem are solved with the unsymmetric multi-frontal method (UMFPACK).

3.1 Newton iteration

The non-linear system of equations resulting from the discretization of the bulk balance equation (2.7)-(2.8) is solved using an incremental iterative Newton-Raphson solution procedure. Dropping the superscript denoting time discretization, we denote the solution at the (sub)iteration step k by $(\mathbf{F}^k, p^k)$, and the incremental growth of the discrete deformation and pressure by $\delta\mathbf{F}^{k+1} = \mathbf{I} + \delta(\nabla\boldsymbol{d}^{k+1}), \delta p^{k+1}$. Since the speed of convergence of Newton's iterations is known to depend on its proper initialization, as initial guess for the iteration process we use $\mathbf{F}^0 = \mathbf{I}$ (the identity matrix), that is, we start from the undeformed geometry. Next, when evolving in time, as initial guess we take the deformation at the previous time step. The problem in its weak form reads: Given an approximation of the solution to (2.7)-(2.8) on the sub-iteration step k, find $\delta\boldsymbol{d}^{k+1}, \delta p^{k+1}$ in an appropriate space of variations, such that

$$\int_{\Omega_o} \mu_1 J_o \nabla(\delta\boldsymbol{d}^{k+1})\mathbf{F}_o^{-1}\mathbf{F}_o^{-T} : \nabla\boldsymbol{\varphi} + p^k[(\mathbf{I} + \nabla\boldsymbol{d}^k)^{-1}\nabla(\delta\boldsymbol{d}^{k+1})]^T : (\mathbf{I} + \nabla\boldsymbol{d}^k)^{-1}\nabla\boldsymbol{\varphi}$$

$$-\delta p^{k+1}\mathrm{Cof}(\mathbf{I} + \nabla\boldsymbol{d}^k) : \nabla\boldsymbol{\varphi} + \int_{\Omega_o} \mu_1 J_o(\mathbf{I} + \nabla\boldsymbol{d}^k)\mathbf{F}_o^{-1}\mathbf{F}_o^{-T} : \nabla\boldsymbol{\varphi} - \mathrm{Cof}(\mathbf{I} + \nabla\boldsymbol{d}^k) : \nabla\boldsymbol{\varphi}p^k = 0$$

$$\int_{\Omega_o} \mathrm{Cof}(\mathbf{I} + \nabla\boldsymbol{d}^k) : \nabla(\delta\boldsymbol{d}^{k+1})q + \int_{\Omega_o} (J^k - 1)q = 0,$$

for all $\boldsymbol{\varphi}, q$. Here $\mathrm{Cof}(\mathbf{M})$ denotes the matrix of cofactors of the generic tensor $\mathbf{M}$, and $\mathbf{F}_o$ does not have superscript since it is taken at the previous time step. Notice that we have used the relation

$$D\mathbf{F}^{-T}(\delta\boldsymbol{d}) = -\mathbf{F}^{-T}(\nabla(\delta\boldsymbol{d}))^T\mathbf{F}^{-T}, \text{ for all } \delta\boldsymbol{d}.$$

The stopping criterion for the algorithm corresponds to

$$\frac{\left\|\delta\boldsymbol{d}^{k+1}\right\|_{H^1(\Omega_o)}}{\left\|\boldsymbol{d}^{k+1}\right\|_{H^1(\Omega_o)}} + \frac{\left\|\delta p^{k+1}\right\|_{L^2(\Omega_o)}}{\left\|p^{k+1}\right\|_{L^2(\Omega_o)}} < tol. \tag{3.5}$$
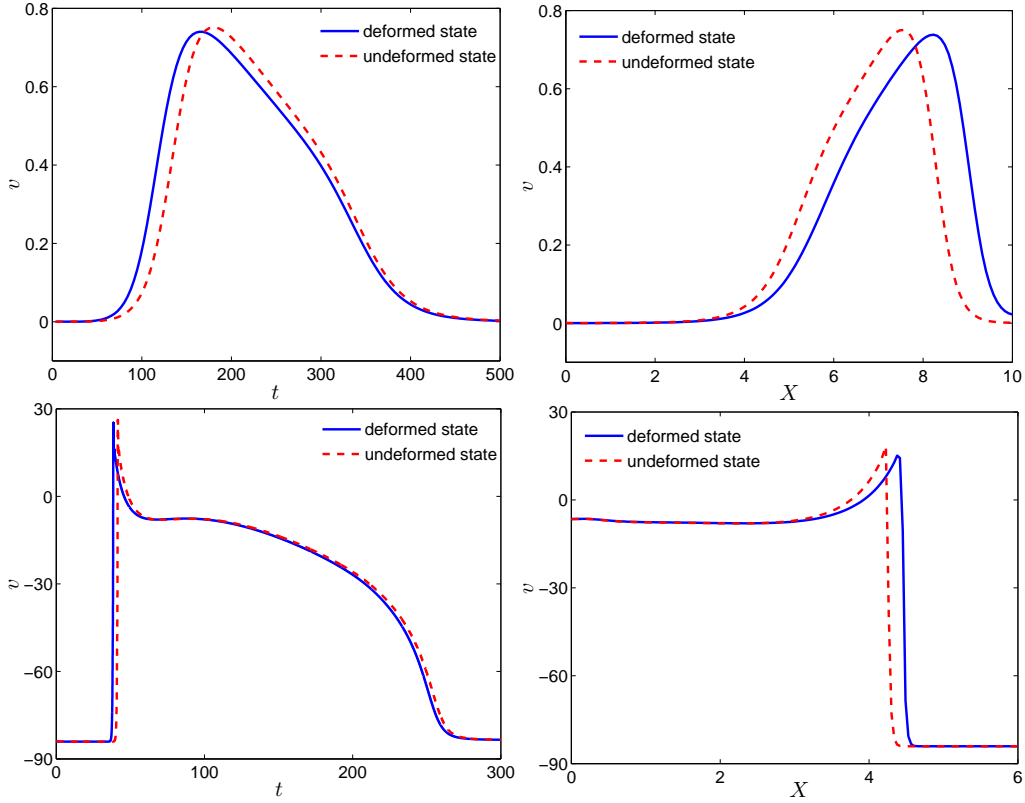
Figure 3: 1D Rogers-McCulloch (top row) and Luo-Rudy (bottom row) monodomain models: Time evolution of the membrane potentials (left column) in the pure electrical propagation (dashed lines) and in the coupling with a description for the contraction of the fiber (solid lines); and potentials' distribution over the fiber (right column).

The sequence $\{\delta \boldsymbol{d}^{k+1}, \delta p^{k+1}\}_k$ ought converge to $(\boldsymbol{d}^{n+1} - \boldsymbol{d}^n, p^{n+1} - p^n)$. Obviously, the cost of each nonlinear iteration is the cost of one residual evaluation and a number of solutions to the linearized subproblems.

4   Numerical Examples

As a sample of our results, we present simulations corresponding to the general systems (2.10) and (2.11) in different scenarios: a single fiber representation, 2D simple geometries, and a truncated ellipsoid in 3D. For the 3D case, our code is based on the C++ object oriented parallel library LifeV [19]. As stated in the previous section, we approximate displacements $\boldsymbol{d}$ with $\mathbb{P}_2$ finite elements, while for the pressure field p and the electrical potential fields $v, u_{\mathrm{i}}, u_{\mathrm{e}}, \boldsymbol{w}$ we use piecewise linear elements. Our main objective now reduces to provide a qualitative insight of the main features of the model.
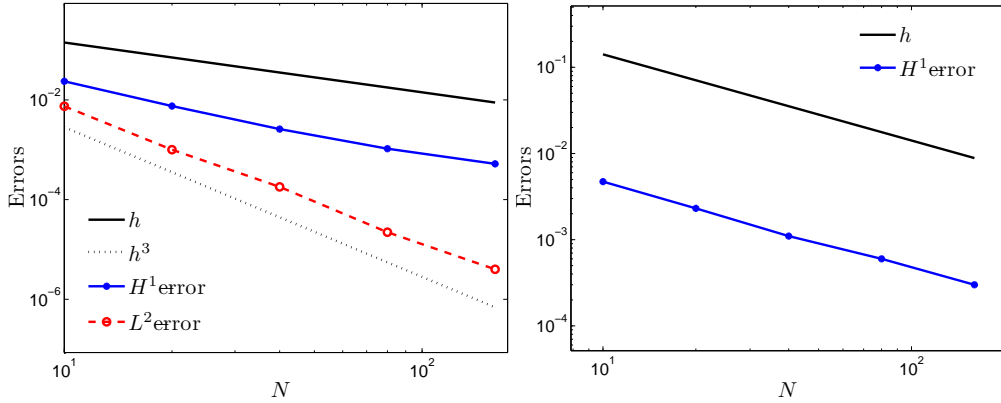
Figure 4: Convergence history for: (left) the displacements in a pure mechanical model problem, and (right) the electrical potential in a pure electrical model problem, on a 2D slab.

4.1 A single fiber simulation

To investigate the propagation of a depolarization wave in a moving domain, consider the system (2.11) for $t > 0$ and $X \in \Omega_o = (0, 1)$. In one spatial dimension, it reduces to solving the following parabolic PDE system

$$\partial_t(v(1 + \gamma)) - D\partial_X((1 + \gamma)^{-1}\partial_X v) = (1 + \gamma)I_{\text{ion}}(v, w)$$
$$\partial_t w = H(v, w),$$

endowed with no-flux boundary conditions. Here I_{ion} and H, when taken as in (2.3), assume the following adimensional parameters (see [28]) $a = 0.13$, $b = 0.013$, $c_1 = 0.26$, $c_2 = 0.1$, $D = 5.6 \times 10^{-3}$. With this choice of parameters, the travelling waves produced have positive speed. Impulse propagation was initiated by application of a stimulus current to the leftmost part of the fiber. The Luo-Rudy kinetics (see the Appendix) are also used in this first test. In Figure 3 we display the time evolution of the transmembrane potential (species v) until the time $t = 300\,\text{ms}$, at the same point in a contractile and fixed fiber (left), and a snapshot of the spatial distribution of v in Ω_o at a fixed time $t = 80\,\text{ms}$ (right). The dashed lines correspond to the propagation of the transmembrane potential on a fixed fiber, while the solid line represents its counterpart in a coupled propagation-contraction of the domain. The representation is done in $X-$coordinates. The situation for both Rogers-McCulloch and Luo-Rudy models is depicted (top and bottom of Figure 3, respectively). From the time evolution plots, it is observed that the electrical potential in a fixed point has a faster variation in a fixed fiber than in a contractile one. This is in well agreement with previous works (as e.g. [34]). On the other hand, the snapshots show that (a pull back to the reference configuration of) the potential wave in a contractile domain travels faster than that on the fixed domain. We stress that this behavior does not imply that in our model the mechanical response precedes the electrical propagation.
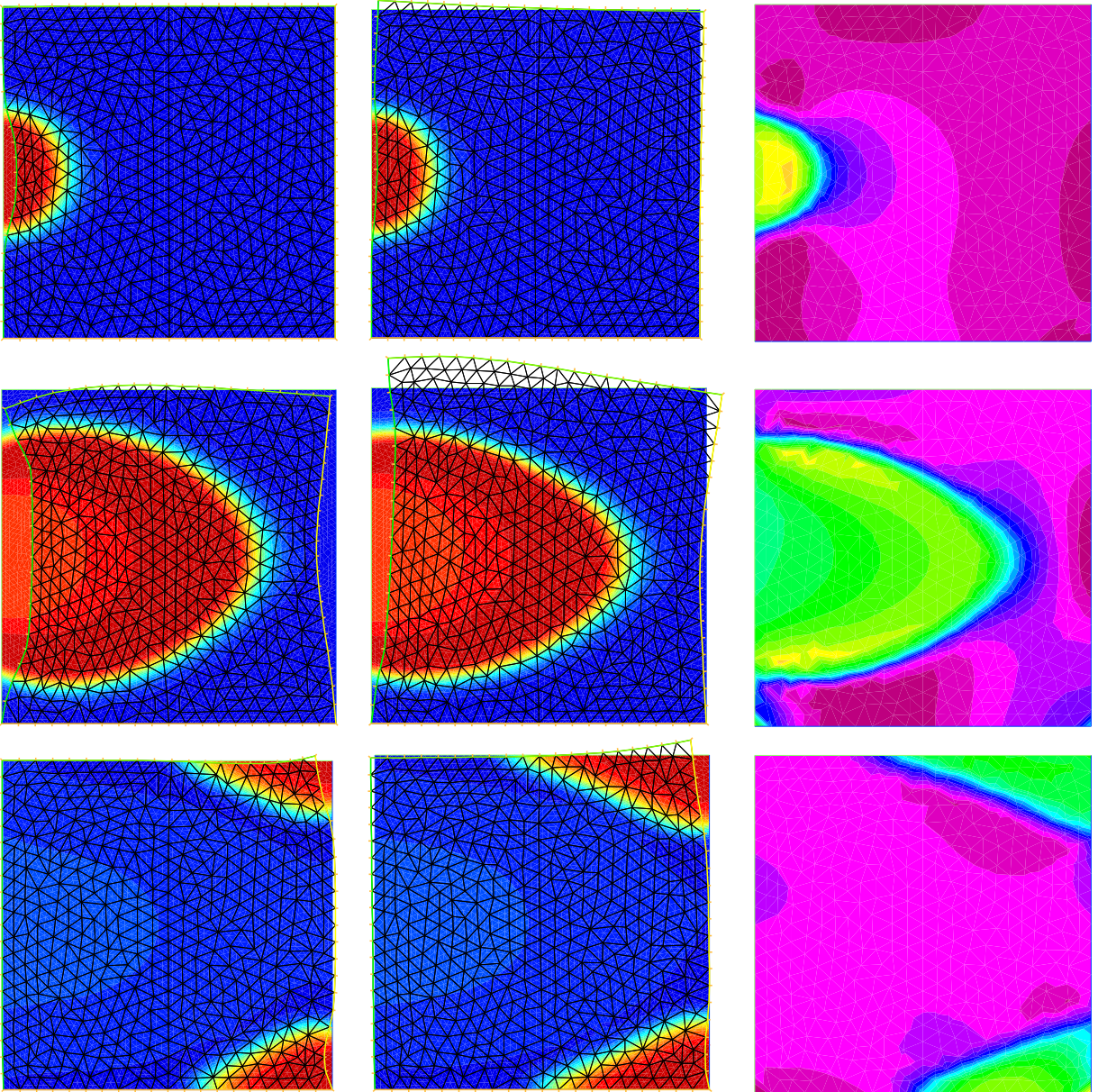
14

Figure 5: 2D Rogers-McCulloch anisotropic monodomain electromechanical coupling: Time evolution of the transmembrane potential and deformed configuration (compared to the resting state) for the compressible model (left), incompressible model (center) and pressure isovalues varying between 33 and 69 (right), for time instants $t = 10\,\mathrm{ms}$ (top), $t = 200\,\mathrm{ms}$ (middle) and $t = 400\,\mathrm{ms}$ (bottom).

4.2 A 2D slab of tissue

In order to validate our *mechanical* numerical scheme (following [24]), we perform one time step iteration, so that all potential fields are known constant quantities acting as initial conditions. The

15

system to solve corresponds to (2.11) on the spatial domain $\Omega_o = (-1, 1)^2$. A simple stretching in the X_1-direction is assumed, along with a compression in the X_2−direction. Let us define $\lambda = 1 + \beta X_1$. The given body force and boundary data (zero displacements on the bottom, and traction on the remaining edges of the slab) are chosen such that the solution of the mechanical problem is $\boldsymbol{d} = (\beta X_1^2/2, X_2(1 + \beta X_1)^{-1} - X_2)^T$, $p = \mu_1/2$ which gives

$$\mathbf{F} = \begin{bmatrix} 1 + \beta X_1 & 0 \\ -X_2(1 + \beta X_1)^{-2} & (1 + \beta X_1)^{-1} \end{bmatrix},$$

and satisfies the incompressibility condition. Analogously, we perform a validation of the *electrical* solver, taking only the simplified monodomain Rogers-McCulloch problem (see e.g. [2]). Dirichlet boundary conditions are imposed on the left and right boundaries of the unit square ($v(0, X_2, t) = 1$ and $v(1, X_2, t) = 1$), and the model parameters are chosen such that the problem possesses the following analytical solution

$$v(X_1, X_2, t) = \left\{ 1 + 0.0001 \exp\left(\sqrt{1/2}(X_1 - C_0 t) \right) \right\}^{-1}.$$

Figure 4 displays the error history for both model problems. We see that (left plot) a convergence of order h^2 is recovered for the displacements in the H^1-norm, while a cubic rate of convergence is achieved in the L^2-norm. For the pure electric problem, a linear convergence is obtained for the electrical potential.

We now consider the anisotropic monodomain electromechanical problem (2.11) on the unit square. We assume that the fibers are aligned with the X_1-axis ($\theta = 0$), so that the conductivity tensor is a diagonal matrix of entries (in Ohm^{-1}cm^{-1}) $D_{11} = \sigma_l = 3.28 \times 10^{-2}$, $D_{22} = \sigma_t = 6.99 \times 10^{-3}$. The membrane model used is the rescaled Rogers-McCulloch (2.4), for which the remaining parameters are $T = 0.63$ ms, $A = 130$ mV, $v_0 = v_{\min} = -84.0$ mV. The initial data for the transmembrane potential and gating variable is

$$v_0(X_1, X_2) = 1 - \left(1 + \exp(-50\sqrt{X_1^2 + (X_2 - 0.5)^2}) \right), \quad w_0(X_1, X_2) = 0.$$

The portion of the boundary where homogeneous Dirichlet boundary conditions for the displacement field are applied is the bottom edge, while the other edges experience no externally applied force. The elastic modulus is $\mu_1 = 4$, the activation parameters are $\beta = 0.3$, $v_{\max} = 26$. The domain is discretized using 4'406 vertices (8'570 triangles), and the time evolution parameters are set to $T_{\text{final}} = 600$ ms, $\Delta t = 1$ms. A tolerance of 1.0×10^{-5} is used for the Newton stopping criterion (3.5), achieving convergence almost always in less than five iterations.

Several experiments have been conducted to obtain a qualitative comparison between the behaviors of the incompressible and nearly compressible formulations. Figure 5 displays snapshots at three different time instants of the potential field and corresponding deformed domain for both models, plus pressure isovalues for the incompressible formulation. As in the 1D simulations, it is observed that the propagation of the electrical wave induces contraction of the tissue. Although the results are somewhat different (in terms of magnitude of the transmembrane potential and displacements), we see that the shown deformations generate strains of reasonable magnitude in both cases, while the pressure field shows no spurious oscillations.
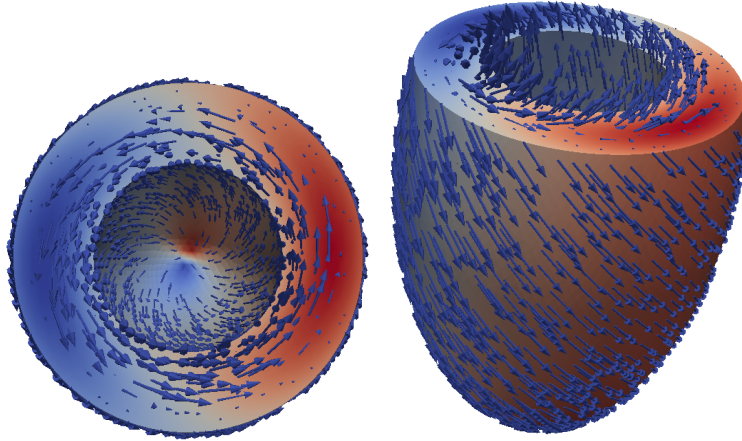
16

Figure 6: Description of the orientation of muscle fibers for an idealized left ventricular geometry.

4.3   A truncated ellipsoidal geometry

Now we illustrate the behavior of the electromechanical coupled model on a idealized left ven-
tricule of height 10cm, discretized using 29'560 nodes forming 155'770 tetrahedra. For our choice
of finite elements, this implies that we handle 222'556 degrees of freedom for the displacements
and 29'560 degrees of freedom for each electrical potential field and gating variable. The domain
is initially subject to a periodic pure-electrical external stimulus. The time discretization parame-
ters are set to $T_{\text{final}} = 600$ms, $\Delta t = 0.5$ms, and the Luo-Rudy kinetics along with the bidomain
model are used to describe the electrical activity. For the orientation of the cardiac fibers, we use
an analytical description given in e.g. [8] (see Figure 6).

As for the initial data, we assume that the tissue is polarized at the beginning of cardiac cycle.
This means that ionic variables are set to zero, while the transmembrane potential corresponds to
constant resting state $v_0 = -84.0$ mV, and we impose an initial stimulus of magnitude 100 mV at
the point $(-0.96, -0.82, -2.5)$. The conductivity parameters (in Ohm^{-1}cm^{-1}) are $\sigma_i^{\text{l}} = 3 \times 10^{-3}$,
$\sigma_i^{\text{t}} = 3.1525 \times 10^{-4}$, $\sigma_e^{\text{l}} = 2 \times 10^{-3}$, $\sigma_e^{\text{t}} = 1.3514 \times 10^{-3}$. The elastic and activation parameters are
set as in the previous subsection. For this example we use the nearly incompressible electrome-
chanical model. From Figure 7, and analogously to the 1D and 2D simulations, a propagation of
the electrical wave is observed, which induces local contraction of the cardiac tissue.

Figure 8 examines the scaling of the solver for the Luo-Rudy bidomain electromechanical
model on a refined ellipsoide (39'850 nodes) at time instant $t = 60$ ms (when the physics of
the coupled problem is already clearly noticeable). The figure provides results in terms of the
number of linear iterations, the average CPU timing for each linear iteration, each preconditioner
computation (built using two layers of overlap), and a single time step. All these accounting for
the resolution of the coupled problem (electrical system plus mechanical system). Up to 64 pro-
cessors, the algorithm shows a reasonable scalable behavior. Since the preconditioner computation
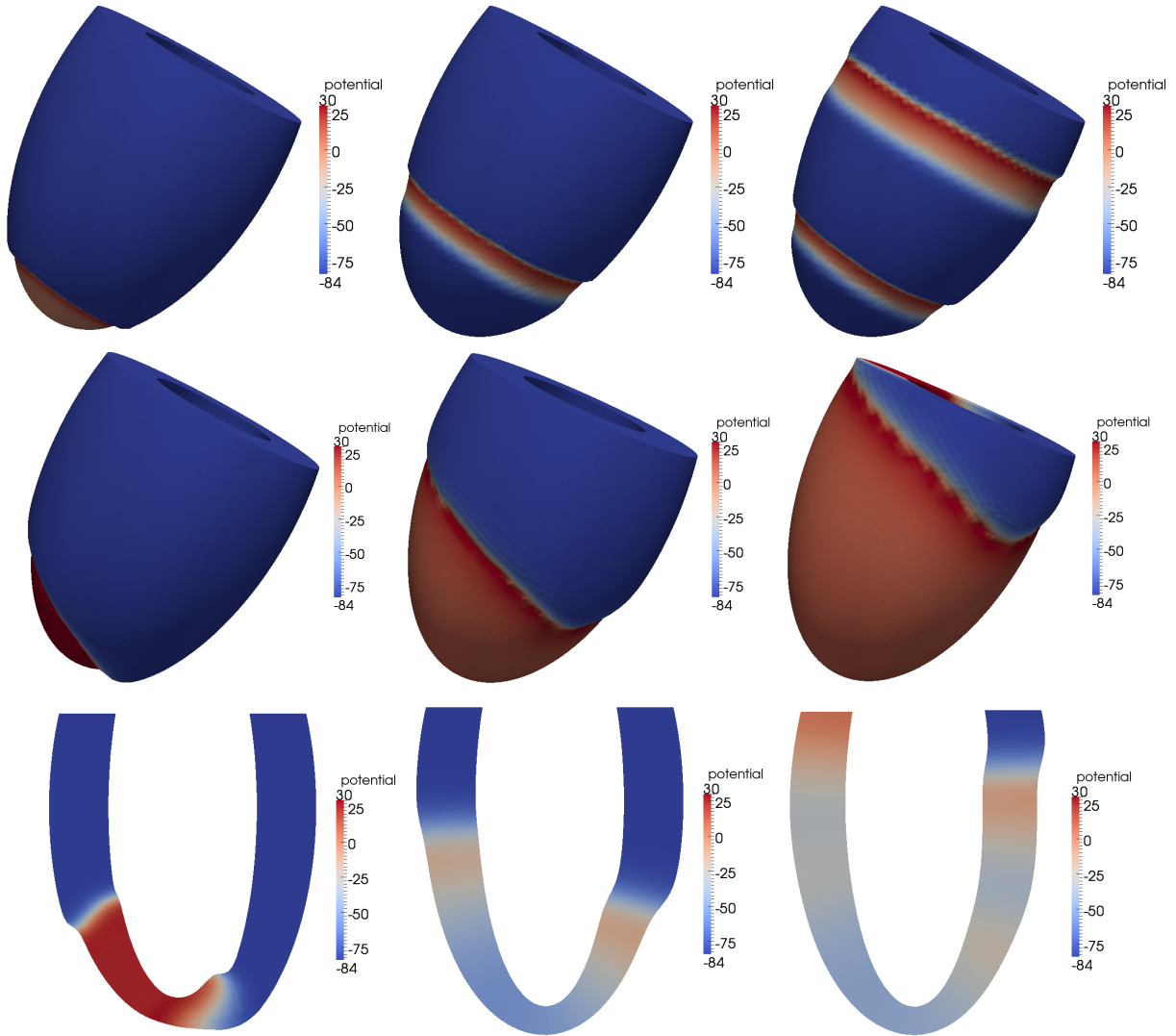takes a no minor part of the overall process, we re-use it.

Figure 7: Snapshots of the evolution of the transmembrane potential and corresponding movement of the mesh, Luo-Rudy I, bidomain electromechanic model on a truncated ellipsoid at time instants $t = 60, 300, 600$ ms (left, middle, right, respectively), in different settings.

4.4 A heart-like geometry

Finally we preform several numerical tests using a 3D bi-ventricular geometry. The associated tetrahedral mesh consists of 13'628 vertices and 69'544 elements. The bidomain Rogers-McCulloch electromechanical model is used here, and Figure 9 illustrates the propagation of the transmembrane potential front, along with the displacement through the cardiac muscle. After the initial activation, a second activation stimulus is applied at $t = 500$ms.
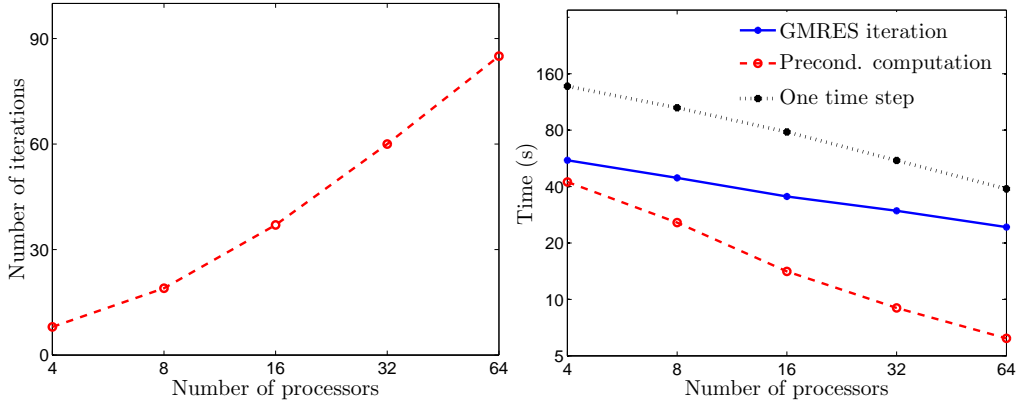
18

Figure 8: Scalability results for the Luo-Rudy bidomain electromechanic model on a truncated ellipsoid at time instant $t = 60$ ms. Number of linear iterations (left) and time spent on different parts of the algorithm (right).

5   Conclusions

In this paper we have proposed a numerical method for a coupled electromechanical model of the cardiac tissue. The electrical part of the model includes a description of the anisotropy in the medium and allows for different electric membrane models. The interaction between the electric and mechanical activity is taken into account by assuming that when decomposing multiplicatively the visible deformation, its active part depends directly on the transmembrane potential through a saturation-like function. In this active part, we also include the anisotropic description of the tissue. The finite element method is based on $\mathbb{P}^2$ elements for the displacements, while for electrical potentials and pressure field we use $\mathbb{P}^1$ elements.

From the modeling point of view, we stress that a deeper understanding of the electromechanical coupling is still needed and open to discussion. As limitations in our treatment, we have neglected several aspects in the modeling of the heart function, such as an accurate anatomical representation of the fiber directions, a model for the blood circulation, Starling effects, a more involved model for the passive mechanical properties of the medium, ionic-scale electromechanics (intracellular calcium handling and cross-bridge formation), etc. Also, the quantitative validation of the model used here implies a difficult task due to the lack of sufficient experimental data. Nevertheless, this work is being extended to consider some of these aspects for current and future studies, with special focus on cases of real pathological interest. For example, cardiac heterogeneities could cause electrical impulses originating from one area of tissue, to fail to conduct into areas with prolonged repolarization [16]. It is also known that in certain myocardiopathies, the electrical potential is able to propagate through all the tissue, while there are specific regions where no contraction takes place. This is a clear application in which cardiac electromechanical models have special interest.

From the numerical viewpoint, several improvements can be rather straightforwardly included in the proposed method. First of all, the time stepping strategy could be upgraded to a adaptive
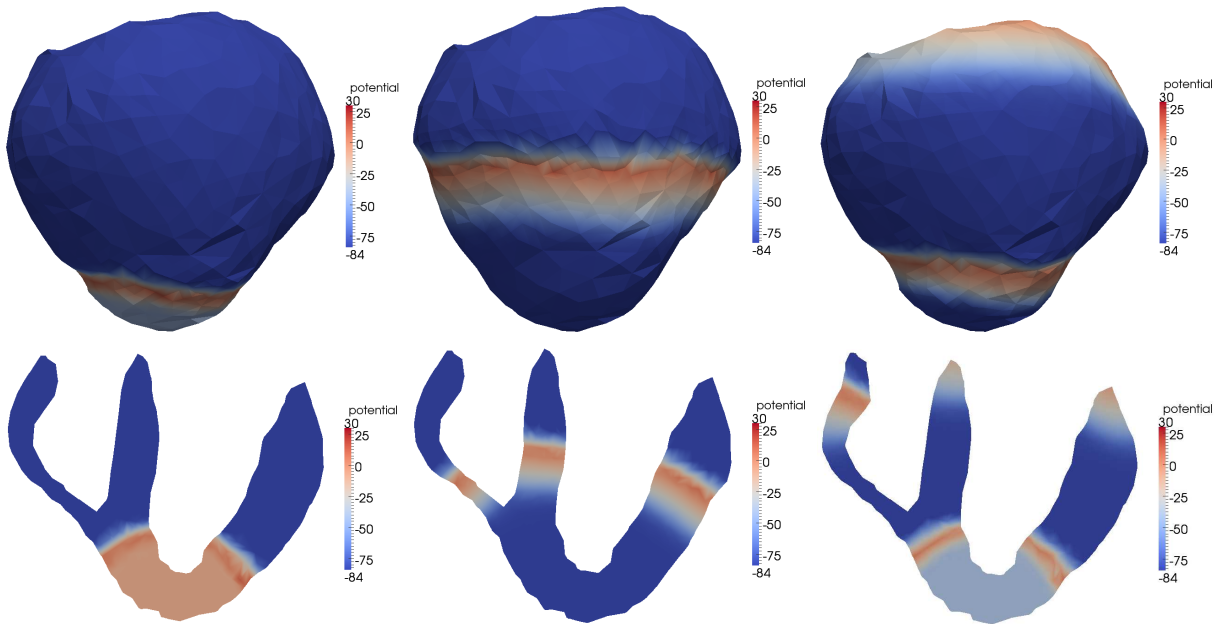
19

Figure 9: Snapshots of the evolution of the transmembrane potential and corresponding slight movement of the mesh, Rogers-McCulloch monodomain electromechanic model at time instants $t = 60, 300, 600$ ms (left, middle, right, respectively).

scheme by using a similar algorithm as the one proposed in [8], where the use of a small time step in the excitation phase would increase the accuracy of capture of the action potential upstroke, while a large time step could be used for the plateau phase. Secondly, other finite element discretizations and more sophisticate preconditioning algorithms can be applied, such as the Monodomain-based block-triangular preconditioning proposed in [11] or structured algebraic multigrid preconditioners in the spirit of [25].

Finally, to the authors' knowledge, the well-posedness analysis, global existence, regularity of solutions, and related questions concerning the mathematical study of cardiac electromechanical models have not been throughly addressed. Although a rigorous analysis in this direction is currently under development [3], we can anticipate that the strong coercivity of the diffusion operators in the fully coupled problems (2.10),(2.11) (which will lead to the performance of a smooth existence analysis) requires a rather complicated development. A way around to this consists in considering a loose coupling between the electrophysiology and mechanical description, which allows us to treat separately the nonlinear elasticity problem following e.g. [5, 18] and the bidomain system as in e.g. [6, 33].

Acknowledgments

A   The Luo Rudy model

We have $I_{\text{ion}}(v, \boldsymbol{w}) = I_{\text{Na}}(v, \boldsymbol{w}) + I_{\text{si}}(v, \boldsymbol{w}) + I_{\text{K}}(v, \boldsymbol{w}) + I_{\text{K}_1}(v, \boldsymbol{w}) + I_{\text{K}_{\text{p}}}(v) + I_{\text{b}}(v)$. The component currents are defined by

$$I_{\text{Na}} = G_{\text{Na}} m^3 h j (v - E_{\text{Na}}), \quad I_{\text{K}_1} = G_{\text{K}_1} K_{1\infty}(v - E_{\text{K}_1}), \quad I_{\text{si}} = G_{\text{si}} l s (v - E_{\text{si}}),$$
$$I_{\text{K}_{\text{p}}} = G_{\text{K}_{\text{p}}} K_{\text{p}}(v - E_{\text{K}_{\text{p}}}), \quad I_{\text{K}} = G_{\text{K}} Y Y_i (v - E_{\text{K}}), \quad I_{\text{b}} = 0.03921(v + 59.87),$$

with $G_{\text{Na}} = 23$, $G_{\text{si}} = 0.07$, $G_{\text{K}} = 0.705$, $G_{\text{K}_1} = 0.604$, $G_{\text{K}_{\text{p}}} = 0.0183$, $E_{\text{Na}} = 54.4$, $E_{\text{K}} = -77$, $E_{\text{K}_1} = -87.26$, $E_{\text{K}_{\text{p}}} = -87.26$, $E_b = -59.87$ (in mV). In addition, $E_{\text{si}} = 7.7 - 13.0287 \ln[\text{Ca}]_+$. The calcium ionic concentration satisfies the Nernst equilibrium

$$d_t[\text{Ca}]_+ = -10^{-4} I_{\text{si}} + G_{\text{si}}(10^{-4} - [\text{Ca}]_+),$$

and all gate variables $\rho \in \{h, j, m, l, s, Y, K_1\}$ evolve according to $d_t \rho = \alpha_\rho(v)(1 - \rho) - \beta_\rho(v)\rho$, which precisely corresponds to the third equation in (2.1). Here, $\alpha_\rho(v)$ and $\beta_\rho(v)$ define the opening and closure rate of the gates, which are given by $\alpha_h = \alpha_j = 0$ for $v \geq -40\,\text{mV}$, $\alpha_h = 0.135 e^{-0.147(v+80)}$ for $v < -40\,\text{mV}$, and

$$\beta_h = \begin{cases} 3.56 e^{0.079v} + 3.1 \times 10^5 e^{0.35v} & \text{for } v < -40\,\text{mV}, \\ (0.13 + 0.13 e^{-0.09(v+10.66)})^{-1} & \text{otherwise}, \end{cases}$$

$$\alpha_j = (v + 37.8)\frac{e^{0.2} + 2.7 \times 10^{-10} e^{-0.04v}}{-7.87 \times 10^{-6}(1 + e^{0.3(v+79.2)})} \quad \text{for } v < -40\,\text{mV},$$

$$\beta_j = \begin{cases} 0.1212 e^{-0.01052v}(1 + e^{-0.1378(v+40.14)})^{-1} & \text{for } v < -40\,\text{mV}, \\ 0.3 e^{-2.535 \times 10^{-7} v}(1 + e^{-0.1(v+32)})^{-1} & \text{otherwise}, \end{cases}$$

$$\alpha_{\text{K}_1} = \frac{1.2}{1 + e^{0.2385(v - E_{\text{K}_1} - 59.215)}}, \quad \alpha_m = \frac{0.32(v + 47.13)}{1 - e^{-0.1(v+47.13)}}, \quad \beta_m = 0.08 e^{-0.0909v},$$

$$\alpha_l = \frac{0.095 e^{-0.01(v-5)}}{1 + e^{-0.072(v-5)}}, \quad \beta_l = \frac{0.07 e^{-0.02(v+44)}}{1 + e^{0.05(v+44)}}, \quad \alpha_s = \frac{0.012 e^{-0.008(v+28)}}{1 + e^{0.15(v+28)}},$$

$$\beta_s = \frac{0.0065 e^{-0.02(v+30)}}{1 + e^{-0.2(v+30)}}, \quad \alpha_Y = \frac{0.0005 e^{0.083(v+50)}}{1 + e^{0.057(v+50)}}, \quad \beta_Y = \frac{0.0013 e^{-0.06(v+20)}}{1 + e^{-0.04(v+20)}},$$

$$\beta_{\text{K}_1} = \frac{0.4912 e^{0.08(v - E_{\text{K}_1} + 5.476)}}{1 + e^{-0.5143(v - E_{\text{K}_1} + 4.75)}} + e^{0.0618(v - E_{\text{K}_1} - 594.31)}.$$

The gating variables Y_i, K_p are assumed to rapidly reach a steady state, and therefore to depend only on the potential u. We set $Y_i(v) = 1$ for $v \leq -100\,\mathrm{mV}$, $K_p = (1 + \mathrm{e}^{0.1672(7.488-v)})^{-1}$, and

$$Y_i = (2.837\mathrm{e}^{0.04(v+77)} - 1)((v + 77)\mathrm{e}^{0.04(v+35)})^{-1} \text{ for } v > -100\,\mathrm{mV}.$$

References

[1] D. Ambrosi, G. Arioli, F. Nobile, A. Quarteroni, The electromechanical coupling in cardiac dynamics, submitted.

[2] M. Bendahmane, R. Bürger, R. Ruiz-Baier, A finite volume scheme for cardiac propagation in media with isotropic conductivities, Math. Comp. Simul. 80 (2010), 1821–1840.

[3] M. Bendahmane, A. Quarteroni, R. Ruiz-Baier, Weak solutions for a coupled model in cardiac electromechanics, in preparation.

[4] M. Boulakia, M.A. Fernández, J.F. Gerbeau, N. Zemzemi, A coupled system of PDEs and ODEs arising in electrocardiograms modeling, Appl. Math. Res. Express (2008), 2–31.

[5] P.G. Ciarlet, Mathematical Elasticity, vol. 1, Three Dimensional Elasticity, North-Holland, Amsterdam, 1998.

[6] Y. Bourgault, Y. Coudière, C. Pierre, Existence and uniqueness of the solution for the bidomain model used in cardiac electro-physiology, Nonlin. Anal. Real World Appl. 10 (2009), 458–482.

[7] C. Cherubini, S. Filippi, P. Nardinocchi and L. Teresi, An electromechanical model of cardiac tissue: Constitutive issues and electrophysiological effects, Prog. Biophys. Molec. Biol. 97 (2008), 562–573.

[8] P. Colli Franzone, L.F. Pavarino, A parallel solver for reaction-diffusion systems in computational electro-cardiology, Math. Models Meth. Appl. Sci. 14 (2004), 883–911.

[9] P. Colli Franzone, G. Savaré, Degenerate evolution systems modeling the cardiac electric field at micro- and macroscopic level, in: A. Lorenzi, B. Ruf (Eds.), Evolution Equations, Semigroups and Functional Analysis, Birkhäuser, Basel, 2002, pp. 49–78.

[10] V. Comincioli, A. Torelli, A mathematical model of contracting muscle with viscoelastic elements, SIAM J. Math. Anal. 19 (1988), 593–612.

[11] L. Gerardo-Giorda, L. Mirabella, F. Nobile, M. Perego, A. Veneziani, A model-based block-triangular preconditioner for the Bidomain system in electrocardiology, J. Comp. Phys. 228 (2009), 3625–3639.

[12] S. Göktepe, E. Kuhl, Electromechanics of the heart: a unified approach to the strongly coupled excitation–contraction problem, Comput. Mech. 45 (2010), 227–243.

[13] G.A. Holzapfel, R.W. Ogden, Constitutive modelling of passive myocardium: a structurally based framework for material characterization, Phil. Trans. R. Soc. A 367 (2009), 3445–3475.

[14] C.O. Horgan, G. Saccomandi, Constitutive models for compressible nonlinearly elastic materials with limiting chain extensibility, J. Elast. 77 (2004), 123–138.

[15] R. Kerckhoffs, P. Bovendeerd, J.C. Kotte, F. Prinzen, K. Smiths, T. Arts, Homogeneity of cardiac contraction despite physiological asynchrony of depolarization: a model study, Ann. Biomed. Engrg. 31 (2003), 536–547.

[16] A.G. Kleber, Y. Rudy, Basic mechanisms of cardiac impulse propagation and associated arrhythmias, Physiol. Rev. 84 (2004), 431–488.

[17] P. Krejčí, J. Sainte-Marie, M. Sorine, J.M. Urquiza, Solutions to muscle fiber equations and their long time behaviour, Nonl. Anal. Real World Appl. 7 (2006), 535–558.

[18] P. Le Tallec, Numerical Methods for Nonlinear Three-dimensional Elasticity. In Handbook of Numerical Analysis, Vol. III, P.G. Ciarlet et Lions eds., North-Holland, 1994.

[19] LifeV library, http://www.lifev.org.

[20] C. Luo, Y. Rudy, A dynamic model of the cardiac ventricular action potential - simulations of ionic currents and concentration changes, Circ. Res. 74 (1994), 1071–1097.

[21] P. Nardinocchi, L. Teresi, On the active response of soft living tissues, J. Elast. 88 (2007), 27–39.

[22] M.P. Nash, A.V. Panfilov, Electromechanical model of excitable tissue to study reentrant cardiac arrhythmias, Prog. Biophys. Molec. Biol. 85 (2004), 501–522.

[23] P. Pathmanathan, J.P. Whiteley, A numerical method for cardiac mechanoelectric simulations, Annals Biomed. Engrg. 37 (2009), 860–873.

[24] P. Pathmanathan, D. Gavaghan, J.P. Whiteley, A comparison of numerical methods used for finite element modelling of soft tissue deformation, J. Strain Anal. 44 (2009), 391–406.

[25] M. Pennacchio, V. Simoncini, Algebraic multigrid preconditioners for the bidomain reaction–diffusion system, Appl. Numer. Math. 59 (2009), 3033–3050.

[26] A. Quarteroni, Numerical models for differential problems. MS&A series Vol. 2, Springer-Verlag, Milan, 2009.

[27] U. Ravens, Mechano-electric feedback and arrhythmias, Prog. Biophys. Molec. Biol. 82 (2003), 255–266.

[28] J.M. Rogers, A.D. McCulloch, A collocation-Galerkin finite element model of cardiac action potential propagation, IEEE Trans. Biomed. Engrg. 41 (1994), 743–757.

[29] J. Sainte-Marie, D. Chapelle, R. Cimrman, M. Sorine, Modeling and estimation of the cardiac electromechanical activity, Comp. & Struct. 84 (2006), 1743–1759.

[30] J.C. Simo, K.S. Pister, Remarks on rate constitutive equations for finite deformations, Comp. Methods Appl. Mech. Engrg. 46 (1984), 201–215.

[31] J. Sundnes, G.T. Lines, X. Cai, B.F. Nielsen, K.-A. Mardal, A. Tveito, Computing the Electrical Activity in the Heart, Springer-Verlag, Berlin, 2006.

[32] T.P Usyk, I.J. LeGrice, A.D. McCulloch, Computational model of three-dimensional cardiac electromechanics, Comput. Visual Sci. 4 (2002), 249–257.

[33] M. Veneroni, Reaction-diffusion systems for the macroscopic Bidomain model of the cardiac electric field, Nonlin. Anal. Real World Appl. 10 (2009), 849–868.

[34] F.J. Vetter, J.M. Rogers, A.D. McCulloch, A finite element model of passive mechanics and electrical propagation in the rabbit ventricles, Comp. Cardiology 25 (1998), 705–708.

[35] J.P. Whiteley, Physiology driven adaptivity for the numerical solution of the Bidomain equations, Annals Biomed. Engrg. 35 (2007), 1510–1520.

[36] J.P. Whiteley, M.J. Bishop, D.J. Gavaghan, Soft tissue modelling of cardiac fibers for use in coupled mechanoelectric simulations, Bull. Math. Biol. 69 (2007), 2199–2225.

MOX Technical Reports, last issues

20/2010 FABIO NOBILE, ALFIO QUARTERONI, RICARDO RUIZ BAIER:
Numerical solution of an active strain formulation for the electro-mechanical activity in the heart

19/2010 LOREDANA GAUDIO, ALFIO QUARTERONI:
hN-adaptive spectral element discretization of optimal control problems for environmental applications

18/2010 PAOLA F. ANTONIETTI, NUR AIMAN FADEL,
MARCO VERANI:
Modelling and numerical simulation of the polymeric extrusion process in textile products

17/2010 ALESSANDRA GUGLIELMI, FRANCESCA IEVA,
ANNA MARIA PAGANONI, FABRIZIO RUGGERI:
A Bayesian random-effects model for survival probabilities after acute myocardial infarction

16/2010 LUCA FORMAGGIA, ANNA SCOTTI:
Positivity and conservation properties of some integration schemes for mass action kinetics

15/2010 ALFIO QUARTERONI, LUCA FORMAGGIA:
Domain Decomposition (DD) methods

14/2010 PAOLA F. ANTONIETTI, LOURENCO BEIRÃO DA VEIGA,
MARCO VERANI:
A Mimetic Discretization of Elliptic Obstacle Problems

13/2010 G.M. PORTA, SIMONA PEROTTO, F. BALLIO:
A Space-Time Adaptation Scheme for Unsteady Shallow Water Problems

12/2010 RICCARDO SACCO, PAOLA CAUSIN, PAOLO ZUNINO,
MANUELA T. RAIMONDI:
A multiphysics/multiscale numerical simulation of scaffold-based cartilage regeneration under interstitial perfusion in a bioreactor

Paolo Biscari, Sara Minisini, Dario Pierotti,
Gianmaria Verzini, Paolo Zunino:
Controlled release with finite dissolution rate